

# Near-Linear Orbit Uncertainty Propagation in the Perturbed Two-Body Problem

Javier Hernando-Ayuso\*, Claudio Bombardelli†, Giulio Baù‡, Alicia Martínez-Cacho§

\**ispace-inc, Tokyo, 113-0007, Japan*

†§*Technical University of Madrid (UPM), Madrid, 28040, Spain*

‡*University of Pisa, Pisa, 56126, Italy*

## Abstract

The paper addresses the problem of minimizing the impact of non-linearities when dealing with uncertainty propagation in the perturbed two-body problem. The recently introduced generalized equinoctial orbital element set (GEqOE) is employed as a means to reduce non-linear effects stemming from  $J_2$  and higher order gravity field harmonics. The uncertainty propagation performance of the proposed set of elements in different Earth orbit scenarios, including low-thrust orbit raising, is evaluated using a Cramér-von Mises test on the Mahalanobis distance of the uncertainty distribution. A considerable improvement compared to all sets of elements proposed so far is obtained.

## 1 Introduction

The ability to rapidly and accurately propagating the probability density function (pdf) of a space object in time is key in space situational awareness (SSA). Tracking an Earth orbiting object through subsequent observation arcs or correctly estimating the probability of collision between two objects sufficiently early in time, for instance, are operations that require an accurate knowledge of the temporal evolution of a pdf.

---

\*Mission Analysis and Flight Dynamics Engineer (in his personal capacity)

†Associate Professor, Space Dynamics Group

‡Assistant Professor, University of Pisa

§PhD student, Space Dynamics Group

The propagation of the pdf that characterizes the uncertainty of the orbital state vector is governed by the Fokker-Plank Equation [1, pp. 192-202]. This partial differential equation is computationally hard to solve, which has motivated the use of approximate methods that can compute the pdf evolution with reasonable accuracy and computational cost. A spectrum of possibilities are available in the literature ranging from very fast but less accurate linear methods to the highly accurate yet computationally expensive Monte-Carlo-based methods. These include Differential Algebra [2], state transition tensors [3, 4], Gaussian Mixture Models [5, 6], unscented transform [7], Polynomial Chaos Expansion [8], Line of Variations [9], Kriging [10]. Combinations of different approaches have also been explored [11]. The common goal of these techniques is to handle the effect of nonlinearities associated with the perturbed orbital motion and resulting in a pdf evolution that can rapidly become far from Gaussian.

Irrespectively of the strategy adopted to tackle nonlinear effects, the choice of the mathematical formulation is a key element when constructing an efficient uncertainty propagation method ([12, 13, 14, 15, 16, 17, 18, 19, 20, 21]). Arguably, before even considering sophisticated algorithms like [2]–[11] one should investigate how to minimize non-linearities that are *intrinsic* to the mathematical structure of the propagated set of ordinary differential equations. A significant step forward in this direction has been made by Arisoff et al. [22], who proposed a set of “ $J_2$  equinoctial orbital elements” (J2EqOE) based on Brouwer-Lyddane’s solution of the main satellite problem. The method allows one to absorb the non-linearities stemming from the  $J_2$  term of the geopotential perturbation and provides a major improvement in uncertainty realism (UR) compared, for example, to classical equinoctial elements.

The purpose of this article is to test the uncertainty propagation performance of yet another set of elements, the generalized equinoctial orbital elements (GEqOE), recently introduced by Baù et al. [23]. Similarly to Arisoff’s elements, GEqOE mitigate the negative effect of  $J_2$  in the propagation of the orbital state. However, there are important differences between the two sets of elements. The first is that GEqOE are related to Cartesian coordinates by transformations expressed in closed analytical form (Sects. 3, 4 in [23]) and evolve according to a set of clearly defined differential equations of motion (Sect. 5 in [23]). The second is that they can be constructed accounting for any perturbation deriving from a potential, not just  $J_2$ . These characteristics make the new set of elements particularly appealing for uncertainty propagation in low-Earth orbit and motivate a detailed analysis of their performance compared to the one of the already proposed J2EqOE.

The article is organized as follows. First a brief review of the generalized orbital motion quantities and the corresponding orbital elements introduced by Baù et al. [23] is provided for convenience. Next, the mathematical treatment of the linear uncertainty propagation in GEqOE is developed. A fully analytical

explanation of the reduction, by use of the proposed elements, of uncertainty propagation nonlinearities associated to secular effects is provided in the subsequent section. Finally, an extensive simulation campaign is conducted to evaluate the UR of the proposed elements compared to competing sets of elements proposed in the literature. The test cases, which include orbits of different eccentricities and inclinations and the impact of low-thrust propulsion, are simulated with a high-fidelity model including high-order geopotential harmonics and third-body effects.

## 2 Generalized Orbital Motion Quantities

Let us consider the perturbed two-body problem written in a geocentric inertial reference frame:

$$\ddot{\mathbf{r}} = -\frac{\mu\mathbf{r}}{r^3} + \mathbf{F}(\mathbf{r}, \dot{\mathbf{r}}, t), \quad (1)$$

where  $\mathbf{r}$ ,  $\dot{\mathbf{r}}$ , and  $\ddot{\mathbf{r}}$  are the geocentric position, velocity, and acceleration, respectively. Moreover,  $r$  is the position magnitude,  $t$  denotes time, and  $\mu$  is the gravitational parameter of the Earth.

Following [23],  $\mathbf{F}$  is split into a term that is derivable from a potential energy  $\mathcal{U}(\mathbf{r}, t)$  and a term  $\mathbf{P}(\mathbf{r}, \dot{\mathbf{r}}, t)$  that is not:

$$\mathbf{F} = \mathbf{P} - \nabla\mathcal{U}. \quad (2)$$

Next, the *total orbital energy*  $\mathcal{E}$  is introduced by adding to the Keplerian energy  $\mathcal{E}_K$  the potential energy  $\mathcal{U}$ :

$$\mathcal{E} = \mathcal{E}_K + \mathcal{U} = \frac{v^2}{2} - \frac{\mu}{r} + \mathcal{U},$$

where  $v$  is the velocity magnitude.

By formally replacing the Keplerian energy with the total energy in the momentum-energy relation as discussed in [23] one obtains the *generalized angular momentum*

$$c = r\sqrt{2\left(\mathcal{E} + \frac{\mu}{r}\right) - u^2} = \sqrt{h^2 + 2\mathcal{U}r^2}, \quad (3)$$

where  $u$  and  $h$  are, respectively, the radial velocity and the osculating angular momentum. This new quantity

can be employed to define the *generalized angular momentum vector* and *eccentricity vector* as, respectively:

$$\begin{aligned}\mathbf{c} &= c \mathbf{e}_h, \\ \mathbf{g} &= \frac{1}{\mu} \mathbf{v} \times \mathbf{c} - \mathbf{e}_r,\end{aligned}$$

where

$$\mathbf{v} = u \mathbf{e}_r + \frac{c}{r} \mathbf{e}_f,$$

is the generalized velocity vector and  $\{\mathbf{e}_r, \mathbf{e}_f, \mathbf{e}_h\}$  is the *orbital* reference frame orthonormal basis.

Denoting by  $g$  the generalized eccentricity, that is  $g = |\mathbf{g}|$ , it is found that  $g, c, \mathcal{E}$  satisfy the relation

$$g = \frac{1}{\mu} \sqrt{\mu^2 + 2\mathcal{E}c^2} = \sqrt{e^2 + \frac{2\mathcal{U}}{\mu^2} (h^2 + 2\mathcal{E}r^2)}, \quad (4)$$

where  $e$  is the osculating eccentricity. The vectors  $\mathbf{c}, \mathbf{g}$  define at any time (as long as  $c \neq 0$ ) a *non-osculating ellipse*  $\Gamma$ , which lies on the orbital plane and has one focus located at the center of mass of the primary body of attraction [23]. The semi-major axis of that conic is the *generalized semi-major axis* ( $a$ ) and is related to the osculating semi-major axis ( $a$ ) by the formula

$$a = -\frac{\mu}{2\mathcal{E}} = a + \frac{\mu\mathcal{U}}{2\mathcal{E}\mathcal{E}_K}. \quad (5)$$

From equations (3), (4), (5) it is immediate to see that  $c, g, a$  coincide with their osculating counterparts  $h, e, a$  when  $\mathcal{U} = 0$ .

Assuming, from now on, that  $\mathcal{E} < 0$ , one can introduce the *generalized mean motion* and *mean anomaly* as, respectively,

$$\nu = \frac{1}{\mu} (-2\mathcal{E})^{3/2}, \quad (6)$$

$$\mathcal{M} = \nu(t - t_p),$$

where  $t_p$  denotes the time of pericenter passage of  $\Gamma$ .

The angular separation between the vectors  $\mathbf{g}$  and  $\mathbf{r}$  defines the *generalized true anomaly*  $\theta$  which can be

obtained from the relations (analogous to the ones holding for the classical true anomaly)

$$\begin{cases} g \cos \theta = \frac{c^2}{\mu r} - 1, \\ g \sin \theta = \frac{cu}{\mu}. \end{cases}$$

Similarly, a *generalized eccentric anomaly*  $G$  can be defined from the relations

$$\begin{cases} g \cos G = 1 - \frac{r}{a}, \\ g \sin G = \frac{ru}{\sqrt{\mu a}}. \end{cases}$$

The *generalized Kepler's equation* takes the form

$$\mathcal{M} = G - g \sin G.$$

Let  $\{\mathbf{e}_X, \mathbf{e}_Y, \mathbf{e}_h\}$  be the classical equinoctial basis introduced in [24]. The angular separation between the vectors  $\mathbf{e}_X$  and  $\mathbf{g}$ , which both lie on the osculating orbital plane, is given by the *generalized longitude of periapsis*

$$\Psi = L - \theta, \tag{7}$$

where

$$L = \omega + \Omega + f \tag{8}$$

is the classical true longitude with  $\omega$  and  $\Omega$  denoting the classical argument of pericenter and right ascension of the ascending node, respectively. By means of the angle  $\Psi$ , one can introduce the *generalized eccentric longitude* and *generalized mean longitudes* as, respectively,

$$\mathcal{K} = G + \Psi, \tag{9}$$

$$\mathcal{L} = \mathcal{M} + \Psi. \tag{10}$$

### 3 Generalized Equinoctial Orbital Elements (GEqOE)

The generalized equinoctial orbital elements (GEqOE) as defined in [23] are constructed on the previously described generalized quantities  $g$  (Eq. 4),  $\nu$  (Eq. 6),  $\Psi$  (Eq. 7), and  $\mathcal{L}$  (Eq. 10). The six elements read:

$$\begin{aligned} \nu, & & p_1 = g \sin \Psi, & & p_2 = g \cos \Psi, \\ \mathcal{L}, & & q_1 = \tan \frac{i}{2} \sin \Omega, & & q_2 = \tan \frac{i}{2} \cos \Omega. \end{aligned}$$

The elements  $p_1, p_2$  represent the projections of the generalized eccentricity vector  $\mathbf{g}$  along the equinoctial basis unit vectors  $\mathbf{e}_Y$  and  $\mathbf{e}_X$ , while the elements  $q_1, q_2$  are two of the classical equinoctial orbital elements [25], where  $i$  is the orbital inclination. Note that when  $\mathcal{U} = 0$ , the generalized equinoctial elements coincide with the alternate equinoctial orbital elements (AEqOE) proposed in [26] and further discussed in Section 5.1.

#### 3.1 Equations of motion

Following [23], the time derivatives of the GEqOE obey

$$\dot{\nu} = -3 \left( \frac{\nu}{\mu^2} \right)^{1/3} \dot{\mathcal{E}}, \quad (11)$$

$$\dot{p}_1 = p_2 \left( \frac{h-c}{r^2} - \frac{\gamma}{h} F_h \right) + \frac{1}{c} \left( \frac{X}{a} + 2p_2 \right) (2\mathcal{U} - rF_r) + \frac{1}{c^2} [Y(r+\varrho) + r^2 p_1] \dot{\mathcal{E}}, \quad (12)$$

$$\dot{p}_2 = p_1 \left( \frac{\gamma}{h} F_h - \frac{h-c}{r^2} \right) - \frac{1}{c} \left( \frac{Y}{a} + 2p_1 \right) (2\mathcal{U} - rF_r) + \frac{1}{c^2} [X(r+\varrho) + r^2 p_2] \dot{\mathcal{E}}, \quad (13)$$

$$\dot{\mathcal{L}} = \nu + \frac{h-c}{r^2} - \frac{\gamma}{h} F_h + \frac{1}{c} \left[ \frac{1}{\alpha} + \alpha \left( 1 - \frac{r}{a} \right) \right] (2\mathcal{U} - rF_r) + \frac{ru\alpha}{\mu c} (r+\varrho) \dot{\mathcal{E}}, \quad (14)$$

$$\dot{q}_1 = \frac{Y}{2h} F_h (1 + q_1^2 + q_2^2), \quad (15)$$

$$\dot{q}_2 = \frac{X}{2h} F_h (1 + q_1^2 + q_2^2), \quad (16)$$

where

$$\dot{\mathcal{E}} = \frac{\partial \mathcal{U}}{\partial t} + uP_r + \frac{h}{r} P_f$$

and

$$X = r \cos L, \quad Y = r \sin L, \quad (17)$$

$$a = \left(\frac{\mu}{\nu^2}\right)^{1/3}, \quad \varrho = \frac{c^2}{\mu}, \quad (18)$$

$$\gamma = Xq_1 - Yq_2, \quad \alpha = \frac{1}{1+\beta}, \quad \beta = \sqrt{1-p_1^2-p_2^2}. \quad (19)$$

Moreover, the terms  $F_r, F_h, P_r, P_f$  in the preceding equations are the projections of  $\mathbf{F}$  and  $\mathbf{P}$  onto the *orbital* reference frame:

$$F_r = \mathbf{F} \cdot \mathbf{e}_r, \quad F_h = \mathbf{F} \cdot \mathbf{e}_h, \quad P_r = \mathbf{P} \cdot \mathbf{e}_r, \quad P_f = \mathbf{P} \cdot \mathbf{e}_f, \quad (20)$$

where the corresponding unit vectors can be conveniently obtained as

$$\mathbf{e}_r = \frac{1}{r}(X\mathbf{e}_X + Y\mathbf{e}_Y), \quad \mathbf{e}_f = \frac{1}{r}(X\mathbf{e}_Y - Y\mathbf{e}_X), \quad \mathbf{e}_h = \mathbf{e}_r \times \mathbf{e}_f.$$

Given the initial position  $\mathbf{r}_0$  and velocity  $\dot{\mathbf{r}}_0$  at some time  $t_0$  expressed in a suitable inertial reference frame  $\Sigma$ , the motion can be propagated to the epoch  $t \neq t_0$  by obtaining the corresponding GEqOE initial conditions (see the conversion formulas in [23], Sect. 3), integrating Eqs. (11–16) and converting back the state expressed in GEqOE at time  $t$  to Cartesian variables (see the conversion formulas in [23], Sect. 4).

## 4 Linear Covariance Propagation in GEqOE

In the following, the linear propagation, by use of the propagated state transition matrix, of the covariance matrix of the GEqOE set is dealt with in details.

Note that in general any of the methods described for pdf propagation in the Introduction can be combined with GEqOE, boosting their performance or reducing their computational cost. Since the objective here is to investigate the suitability of GEqOE for orbital uncertainty propagation, nonlinear methods are out of the scope of this work.

### 4.1 State Transition Matrix Propagation

Equations (11)–(16) can be written as

$$\dot{\mathbf{y}} = \mathbf{f}(\mathbf{y}, t), \quad (21)$$

where  $\mathbf{y} = (\nu, p_1, p_2, \mathcal{L}, q_1, q_2)^T$  denotes the state vector in GEqOE.

An orbit  $\mathbf{y}(t)$  close to a reference orbit  $\mathbf{y}_*(t)$  can be propagated linearly in time from an initial epoch  $t_0$  as

$$\mathbf{y}(t) \approx \mathbf{y}_*(t) + \Phi(t, t_0)(\mathbf{y}(t_0) - \mathbf{y}_*(t_0)),$$

where the reference orbit state transition matrix  $\Phi$  is the solution of the linear Cauchy problem

$$\begin{cases} \frac{\partial \Phi}{\partial t} = \frac{\partial \mathbf{f}}{\partial \mathbf{y}}(\mathbf{y}_*(t), t) \Phi, \\ \Phi(t_0, t_0) = I, \end{cases} \quad (22)$$

with  $I$  the  $6 \times 6$  identity matrix. The matrix  $\partial \mathbf{f} / \partial \mathbf{y}$  can be computed analytically for the GEqOE as described in Appendix A.

## 4.2 Linear Covariance Propagation and Nonlinear Mapping into Cartesian Coordinates

The state transition matrix  $\Phi(t, t_0)$  can be employed for the linear covariance matrix propagation in GEqOE space,  $P_{\mathbf{y}}$ , as

$$P_{\mathbf{y}}(t) = \Phi(t, t_0) P_{\mathbf{y}}(t_0) \Phi^T(t, t_0).$$

In practice, the GEqOE covariance matrix at  $t_0$  can be obtained starting from the corresponding covariance matrix,  $P_{\mathbf{x}}$ , in another set of coordinates  $\mathbf{x}$  (e.g. Cartesian elements) by the linear mapping

$$P_{\mathbf{y}}(t_0) = J(t_0) P_{\mathbf{x}}(t_0) J^T(t_0), \quad J = \frac{\partial \mathbf{y}}{\partial \mathbf{x}}. \quad (23)$$

The Jacobian matrix  $J$  for the case of Cartesian coordinates is given in [23], Sect. 6.2.

After linearly propagating  $P_{\mathbf{y}}(t)$  until epoch  $t$ , the uncertainty cloud can be mapped back to Cartesian coordinates by a full *nonlinear* transformation employing the element conversion equations in [23], Sect. 4. The whole scheme, which provides a very efficient method for propagating an initial uncertainty cloud is depicted in Figure 1. It will be shown, in the remainder of this article, that this procedure is particularly resilient against perturbation-driven nonlinear effects hence preserving the UR of the distribution for a longer timespan compared to other methods.



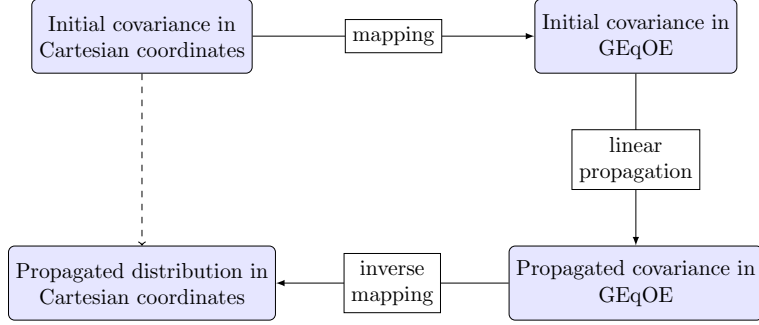


Figure 1: Uncertainty propagation scheme.

## 5 Mitigation of Nonlinear Effects

In this section a simple mathematical explanation is provided to demonstrate the ability of the newly proposed uncertainty propagation method to minimize UR losses.

### 5.1 Keplerian motion

As detailed in [26], when an element-based representation, such as classical equinoctial elements, is employed, five of the six coordinates evolve linearly (they are actually constant) under Keplerian orbital motion while the evolution of the time-element coordinate (the mean longitude, in the case of classical equinoctial elements) is not exactly linear with respect to the other state elements.

After indicating with  $a_*$  the initial (reference) semi-major axis,  $\ell$  the mean longitude, and assuming an initial uncertainty in the semi-major axis  $\varepsilon_0^a$ , the time evolution of the uncertainty-affected mean longitude for a Keplerian orbit obeys

$$\ell(t) = \ell_0 + \sqrt{\frac{\mu}{(a_* + \varepsilon_0^a)^3}}(t - t_0), \quad (24)$$

which yields a *secular* growth of the mean longitude uncertainty:

$$\varepsilon^\ell(t) = \ell(t) - \ell(t)|_{\varepsilon_0^a=0} = \left( -\frac{3}{2a_*}\varepsilon_0^a + \frac{15}{8a_*^2}(\varepsilon_0^a)^2 + O((\varepsilon_0^a)^3) \right) n_*(t - t_0), \quad (25)$$

where  $n_*(t - t_0)$  is the accumulated mean longitude difference for the nominal (uncertainty free) orbit since the initial epoch and  $n_*$  is the mean motion of that nominal orbit.

Equation (25) shows that a linear propagation of a pdf expressed in classical equinoctial elements will be imprecise as a result of the truncation error, growing linearly in time, in the propagation of the mean longitude.

As originally proposed by [26], the classical equinoctial elements can be improved by employing the mean motion as an element in place of the semi-major axis. The resulting elements, coined “alternative equinoctial orbital elements” (AEqOE), are effective against the above-mentioned nonlinear truncation error.

If the pdf is expressed with respect to AEqOE, an initial uncertainty in the mean motion variable  $\varepsilon_0^n$  corresponds to

$$\ell(t) = \ell_0 + (n_* + \varepsilon_0^n)(t - t_0), \quad (26)$$

$$\varepsilon^\ell(t) = \varepsilon_0^n(t - t_0), \quad (27)$$

providing a time evolution of the mean longitude uncertainty that is perfectly linear with respect to the initial mean motion uncertainty.

## 5.2 $J_2$ -induced Secular Perturbations

Let us now consider the case of a perturbed orbital motion whose perturbing force is fully derivable from a potential. In particular, let us consider the effect of the  $J_2$  term of the gravity field harmonics. Analogously to the previous section, we assume an initial semi-major axis uncertainty  $\varepsilon_0^a$ .

If the orbital motion is represented in AEqOE, the assumed semi-major axis uncertainty corresponds to a mean motion uncertainty

$$\varepsilon_0^n = -\frac{3}{2}\sqrt{\frac{\mu}{a^5}}\varepsilon_0^a + O((\varepsilon_0^a)^2).$$

On the other hand, if the orbital motion is represented in GEqOE, it is possible to show that the assumed semi-major axis uncertainty corresponds to a generalized mean motion uncertainty

$$\varepsilon_0^\nu = -\frac{3}{2}\sqrt{\frac{\mu}{a^5}}\varepsilon_0^a + O_2(\varepsilon_0^a, J_2).$$

The previous uncertainties  $\varepsilon_0^n$ ,  $\varepsilon_0^\nu$  are equal to first order in  $\varepsilon_0^a$ . However, their nonlinear contribution to the evolution of the, respectively, mean motion and generalized mean motion errors, will be here shown to be different.

Following [27], the expression of the disturbing function after averaging over one orbital period reads

$$\overline{\mathcal{R}} = \frac{J_2 R^2 n^2}{4(1 - e^2)^{3/2}}(2 - 3 \sin^2 i),$$

where, without complicating the notation,  $e$ ,  $i$ , and  $n$  stand here for the mean values of eccentricity, inclination, and mean motion, respectively. The mean rate of the mean longitude can be derived from Lagrange’s

planetary equations for  $-n\tau$  (with  $\tau$  the time of pericenter passage) wherein the disturbing function is replaced by  $\overline{\mathcal{R}}$  (see [27]):

$$\dot{\ell} = n + \frac{J_2 R^2 n^{7/3}}{\mu^{2/3}} \lambda(e, i), \quad (28)$$

with

$$\lambda = \frac{3}{2(1-e^2)^2} \left[ (1 + \sqrt{1-e^2}) \left( 1 - \frac{3}{2} \sin^2 i \right) + \cos^2 i - \cos i \right].$$

Note that  $n$  and  $i$  are constant (there are no secular nor long-period variations of these elements under  $J_2$  [28]) while  $e$  is constant after neglecting  $J_2$ -induced long-period effects.

Let us consider, for simplicity, the case of a circular equatorial orbit ( $i = 0$ ,  $e = 0$ ) and introduce the notation

$$A = \frac{3R^2}{2\mu^{2/3}}. \quad (29)$$

Integration of equation (28) yields

$$\ell = \ell_0 + n(t - t_0)(1 + 2n^{4/3} J_2 A). \quad (30)$$

After writing the mean motion as the sum of its nominal value and the associated error:

$$n = n_* + \varepsilon_0^n,$$

and by developing  $n^{4/3}$  (in Eq. 30) in Taylor series with respect to  $\varepsilon_0^n$ , the mean longitude error can be obtained as

$$\varepsilon^\ell = (t - t_0) \left[ \left( 1 + \frac{14}{3} J_2 A n_*^{4/3} \right) \varepsilon_0^n + \left( \frac{28}{9} J_2 A n_*^{1/3} \right) (\varepsilon_0^n)^2 + O((\varepsilon_0^n)^3) \right], \quad (31)$$

which is characterized by a secular growth with a *nonlinear* dependency on the mean motion error due to the  $J_2$  term.

A similar analysis can be developed for a formulation based on GEqOE. When the GEqOE are employed, the generalized mean motion state variable  $\nu$  is a constant in the  $J_2$ -only perturbed two-body problem. Moreover, for an equatorial orbit the potential energy associated with the  $J_2$  term yields

$$\mathcal{U} = -\frac{J_2 \mu R^2}{2r^3}, \quad (32)$$

and the time derivative of the generalized mean longitude becomes (Eq. 14)

$$\dot{\mathcal{L}} = \nu_0 + \frac{h - c}{r^2} + \frac{J_2 \mu R^2}{2cr^3} \left[ \frac{1}{\alpha} + \alpha \left( 1 - \frac{r}{a_0} \right) \right], \quad (33)$$

where  $\alpha$  has been defined in (19) and  $\nu_0$ ,  $a_0$  are the constant values taken by the generalized mean motion and semi-major axis along the solutions.

Noting from Eqs. (3), (32) that

$$\frac{h - c}{r^2} = \frac{J_2 \mu R^2}{2cr^3} + O(J_2^2), \quad (34)$$

the secular variation (to first order in  $J_2$ ) in generalized mean longitude for a circular equatorial orbit is given by (see Appendix B)

$$\mathcal{L} = \mathcal{L}_0 + \nu_0(t - t_0)(1 + J_2 A \nu_0^{4/3}). \quad (35)$$

Writing the generalized mean motion as the sum of its (constant) nominal value and the associated error:

$$\nu_0 = \nu_* + \varepsilon_0^\nu,$$

and expanding  $\nu_0^{4/3}$  (in Eq. 35) in Taylor series with respect to  $\varepsilon_0^\nu$  yields the generalized mean longitude error

$$\varepsilon^{\mathcal{L}} = (t - t_0) \left[ \left( 1 + \frac{7}{3} J_2 A \nu_*^{4/3} \right) \varepsilon_0^\nu + \left( \frac{14}{9} J_2 A \nu_*^{1/3} \right) (\varepsilon_0^\nu)^2 + O((\varepsilon_0^\nu)^3) \right]. \quad (36)$$

After comparing Eq. (31) with Eq. (36) there appears to be a reduction by a factor of two for the nonlinear dependency on the mean motion error. This means that the use of GEqOE has absorbed half of the  $J_2$  nonlinear secular effect on the mean longitude. Indeed, simple tests for circular equatorial orbits have confirmed an improvement of UR by a factor very close to two. Extending the present analytical treatment to the much more complex case of non-circular and non-equatorial orbits is out of the scope of the present article.

## 6 Results

To assess the efficiency of the orbital uncertainty propagation using the GEqOE set, a Cramér-von Mises (CvM) test of the Mahalanobis distance distribution is used following the recent work of Aristoff et al. [22]. This test evaluates whether a covariance matrix, based on a chosen set of coordinates, is likely to represent the true covariance. For convenience, the process is briefly described in Algorithm 1. More details can be found in [22].

The first step is to propagate the covariance matrix in the coordinates set of interest. A linear propagation of that matrix can be adopted for simplicity.

Subsequently, a sufficiently large set ( $N = 10000$  for these results) of orbital states sampled from the initial covariance are propagated with a high-fidelity orbital dynamics model in Cartesian coordinates and converted into the set of variables being evaluated. For each epoch, the Mahalanobis distance  $\mathfrak{m}$  of each sample is calculated using the linearly propagated covariance and the propagated state of the sample. If the true pdf is Gaussian, then the Mahalanobis distance will follow a chi-squared distribution with 6 degrees of freedom, whose cumulative distribution function (cdf) is

$$F(z) = 1 - \frac{1}{8} \exp\left(-\frac{z}{2}(z^2 + 4z + 8)\right). \quad (37)$$

The CvM test statistics is calculated by comparing this cdf with the empirical cumulative distribution function of the true distribution. If the CvM test is satisfied, the two cdf are found to agree and one can say that the covariance is realistic.

---

**Algorithm 1** Cramér-von Mises test

---

```

1:  $P_{\mathbf{y}}(t) = \Phi(t, t_0) P_{\mathbf{y}}(t_0) \Phi^T(t, t_0)$  ▷ covariance matrix linear propagation
2: for  $i = 1, \dots, N$  do
3:    $\mathbf{x}_i(t_0)$  ▷ initial covariance sampling
4:    $\mathbf{x}_i(t)$  ▷ true orbit of the sample propagation
5:    $\mathbf{y}_i(t) = \mathbf{y}(\mathbf{x}_i(t), t)$  ▷ conversion to state variables being tested
6: end for
7:  $\boldsymbol{\mu}_{\mathbf{y}}(t) = \frac{1}{N} \sum_i^N \mathbf{y}_i(t)$  ▷ true mean orbit
8: for  $i = 1, \dots, N$  do
9:    $\mathfrak{M}_i(\mathbf{y}_i; \boldsymbol{\mu}_{\mathbf{y}}, P_{\mathbf{y}}) = (\mathbf{y}_i - \boldsymbol{\mu}_{\mathbf{y}})^T P_{\mathbf{y}}^{-1} (\mathbf{y}_i - \boldsymbol{\mu}_{\mathbf{y}})$  ▷ Mahalanobis distance
10: end for
11:  $Q = \frac{1}{12N}$  ▷ CvM test statistics initialization
12: for  $j = 1, \dots, N$  do ▷ in increasing order of the Mahalanobis distance
13:    $Q = Q + \left(\frac{2j-1}{2N} - F(\mathfrak{M}_j)\right)^2$  ▷  $F$  is the cdf of a 6D chi-squared
14: end for
15: if  $Q < Q^* \simeq 1.16$  then
16:   covariance is realistic
17: end if

```

---

The Cramér-Von Mises test is applied to the proposed GEqOE formulation. For comparison, results for the J2EqOE elements recently proposed by Aristoff et al. [22] and for the alternative equinoctial elements (AEqOE) [26] are also computed.

Table 1: Initial orbital elements for Cases 1, 2, 3. Angles are in degrees.

	$a$ (km)	$e$	$i$	$\Omega$	$\omega$	$M$
1)	7136.6	0.00949	72.9	116	57.7	105.5
2)	26628.1	0.742	63.4	120	0	144
3)	38200.0	0.8167539267	25	120	0	0

The following three different test cases are analyzed:

Case 1) LEO from [22],

Case 2) High-Earth orbit (HEO) from [22],

Case 3) super Geostationary transfer orbit (super-GTO).

For each of these three test cases two scenarios are investigated: (a) a ballistic scenario and (b) a constant low-thrust tangential acceleration scenario. The low-thrust-perturbed scenarios are defined based on mega-constellation LEO satellites (Case 1) and all-electric satellites maneuvered to GEO (Cases 2 and 3). The employed control law sets the thrust vector tangent to the nominal trajectory and with constant magnitude. Note that in practical applications new measurements are performed leading to a continuous update of the covariance statistics readily available to the owner/operator of a specific satellite and possibly distributed to other parties as well. Nevertheless, it is still relevant to study how such covariance would evolve without considering new measurements in case these updates were not available.

For the LEO case, the thrust magnitude and the spacecraft mass are set to 15 mN and 260 kg, respectively, based on realistic estimates for Starlink satellites<sup>1</sup>. For the HEO and super-GTO, 165 mN and 2200 kg were used in line with published figures for the Eutelsat 115 West B satellite<sup>2</sup>.

The initial orbital conditions are shown in Table 1, where all the elements are expressed in the Earth-centered J2000 frame. The initial epoch is 2021 October 20 00:00:00 TDB and the initial covariance in equinoctial orbital elements (EqOE)<sup>3</sup> is given in Table 2.

The sampled states are propagated using Matlab’s ode113 (Adams–Bashforth–Moulton predictor corrector method with variable order between 1 and 13), while the predictions of the nominal state and the associated

<sup>1</sup>A nominal 260 kg wet mass has been assumed based on NASA Space Science Data Coordinate Archive (<https://nssdc.gsfc.nasa.gov/nmc/spacecraft/display.action?id=2019-074D>). In addition, a roughly estimated 15 mN thrust after fitting TLE data of Starlink satellites during their spiral up phase has been considered.

<sup>2</sup>Based on TLE data, Eutelsat 115 West B was boosted from a  $\approx 70000$  km apogee super-GTO to a GEO from March to October 2015. The satellite employed a XIPS-25 propulsion system of  $\approx 165$  mN maximum thrust capability with an estimated wet mass of 2200 kg [29].

<sup>3</sup>Note that  $P_1, P_2, \ell$  are the osculating orbital elements corresponding to  $p_1, p_2, \mathcal{L}$  of GEqOE, and coincide with them if  $\mathcal{U} = 0$ .

Table 2: Initial covariance in EqOE for Cases 1, 2, 3.

	$\sigma_a$ (km)	$\sigma_{P_1}$	$\sigma_{P_2}$	$\sigma_{q_1}$	$\sigma_{q_2}$	$\sigma_\ell$ (deg)
1)	20	$10^{-3}$	$10^{-3}$	$10^{-3}$	$10^{-3}$	$10^{-2}$
2)	2	$10^{-4}$	$10^{-4}$	$10^{-4}$	$10^{-4}$	$\frac{7}{900}$
3)	2	$10^{-4}$	$10^{-4}$	$10^{-4}$	$10^{-4}$	$\frac{7}{900}$

covariance matrix are carried out with a Runge-Kutta method of 4th order and a time step close to 60 seconds. To this end, the state transition matrix in GEqOE is computed using the variational equations provided in Appendix A. Instead, for AEqOE and J2EqOE the state transition matrix is computed from that in GEqOE using the Jacobian of the corresponding transformation.

All scenarios consider luni-solar gravitational perturbations as forces not included in the potential energy defining the GEqOE, as recommended in [23]. The position of these celestial bodies are obtained from the JPL DE430 ephemeris. The Earth gravitational field is modeled following Grace gravity model 05 GGM05C [30] truncated to the 8th degree and order, and all its terms except for the point mass potential are included in the potential energy  $\mathcal{U}$ . The Earth-centered Earth-fixed coordinate system (ECEF) is set as ITRF93. The calculation of the Earth gravitational potential, its gradient and Hessian in ECEF are performed following the method of Cunningham and Metris [31, 32]. The details about the procedure used to include the Earth gravitational potential in the GEqOE formulation are described in Appendix C.

Figure 2 shows the CvM test statistics as a function of time for the no-thrust scenario of Case 1. This case was analyzed by Aristoff et al. [22] and features a relatively-low initial orbit accuracy (see Table 2). As Aristoff et al. showed, the J2EqOE formulation can represent the real orbit uncertainty longer than simpler methods that do not account for the  $J_2$  perturbation like AEqOE. In particular, the CvM test fails before 6 orbital periods in J2EqOE, and before 2 orbital periods for AEqOE. The new proposed GEqOE formulation can further extend the covariance realism to almost 8 orbits.

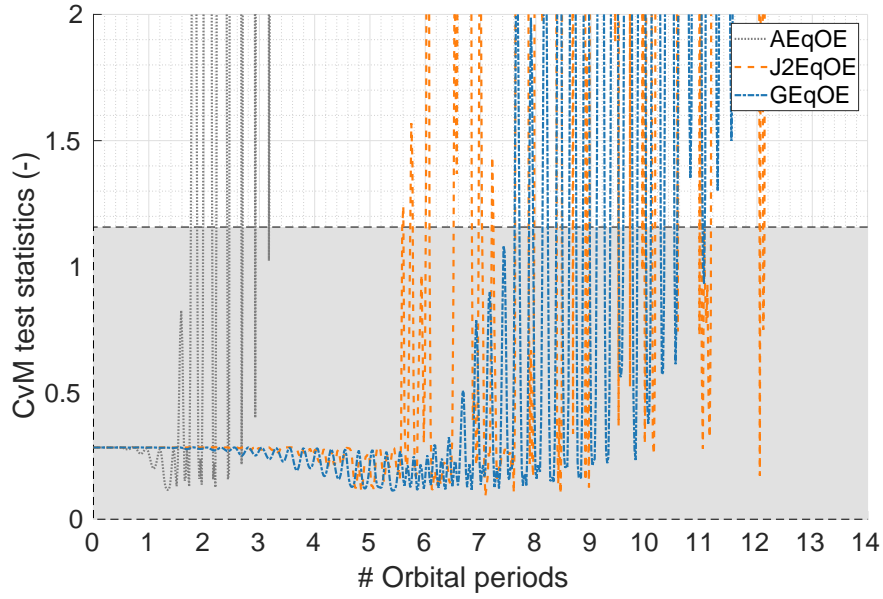


Figure 2: CvM test statistics for Case 1 (ballistic).

The UR improvement of the GEqOE formulation can be partly reduced if a significant acceleration that cannot be included in the potential energy  $\mathcal{U}$  perturbs the trajectory. Nevertheless, in spite of the fact that such reduction is more significant for GEqOE compared to the AEqOE and J2EqOE formulations (see Fig. 3), the former is still able to stay Gaussian longer than the other two.

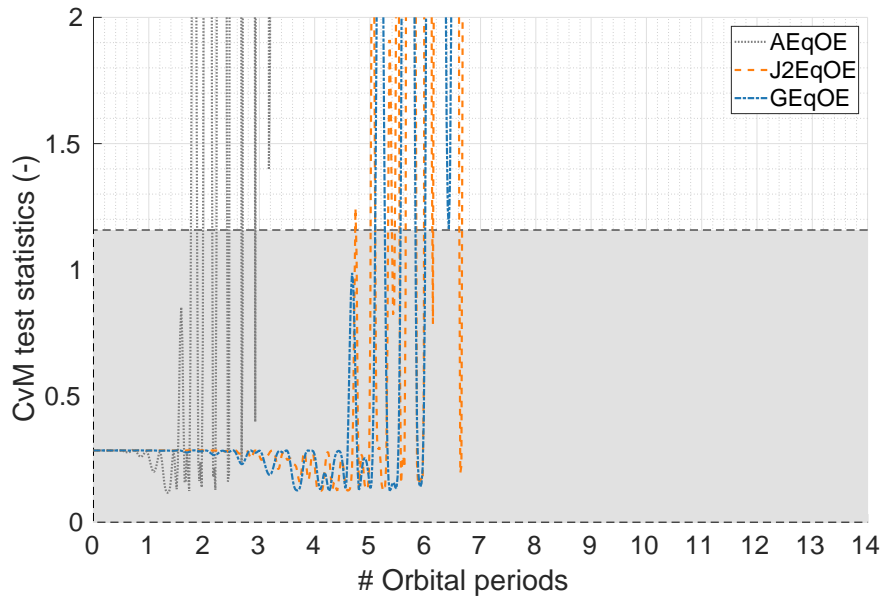


Figure 3: CvM test statistics for Case 1 (low-thrust).



Ballistic Case 2 was also analyzed by Aristoff et al. [22], and it was pointed out that the realism was lost near the periapses. This was confirmed by our simulations as seen in Fig. 4. AEqOE loses realism after a few orbits, while it takes more than 10 revolutions for J2EqOE. Remarkably, using a GEqOE formulation, the UR can be prolonged for more than 30 orbits in this case.

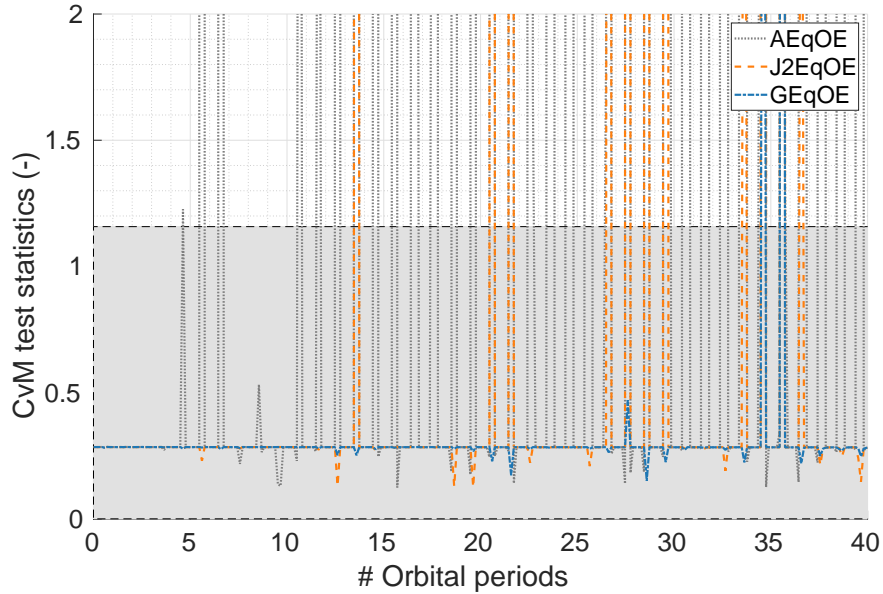


Figure 4: CvM test statistics for Case 2 (ballistic).

Figure 5 shows the effect of adding a tangential thrust to Case 2. The three formulations can only accurately describe the real uncertainty for shorter periods of time, but, still, the GEqOE formulation increases the realism by about 4 orbits compared to the J2EqOE one.

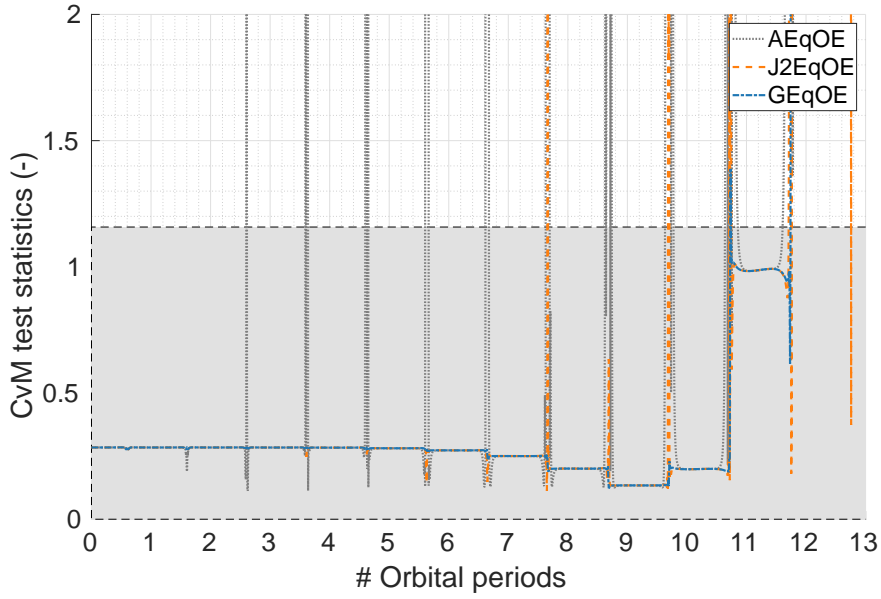


Figure 5: CvM test statistics for Case 2 (low-thrust).

The results for Case 3 are shown in Figs. 6 and 7 for the ballistic and low-thrust scenarios, respectively. The results are similar to the previous case and GEqOE shows better performance than the other methods. In particular, the covariance realism is conserved for about 29 orbits compared to the 11 orbits of J2EqOE in the absence of thrust. If the propulsion system is active through the propagation period, GEqOE (10 orbits) can still better predict the distribution than J2EqOE (8 orbits).

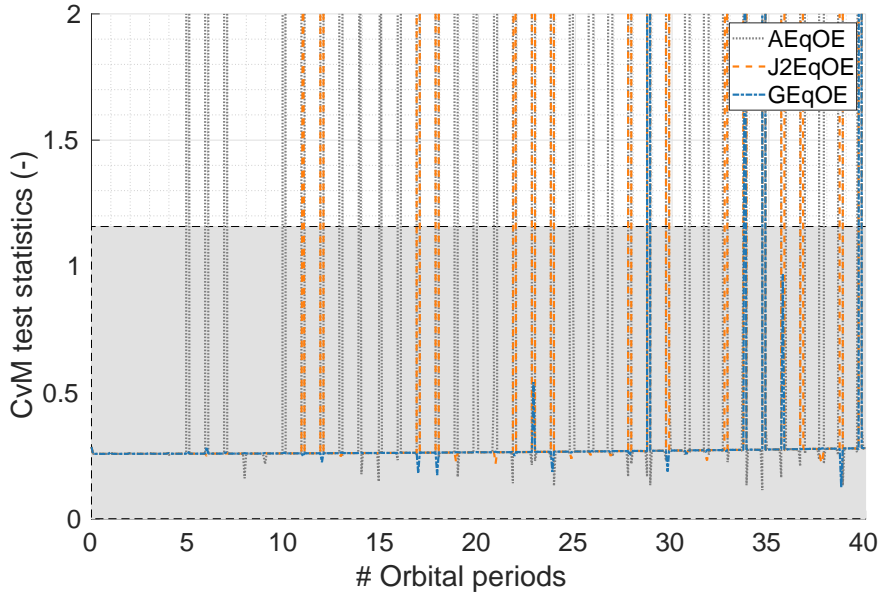


Figure 6: CvM test statistics for Case 3 (ballistic).

Table 3: Number of revolutions for the CvM test before failure.

Case/Scenario	AEqOE	J2EqOE	GEqOE	GEqOE(J <sub>2</sub> )
1/a (LEO, ballistic)	1.77	5.60	7.62	5.67
1/b (LEO, low-thrust)	1.77	4.74	5.11	4.66
2/a (HEO, ballistic)	4.62	13.60	34.61	13.60
2/b (HEO, low-thrust)	2.60	7.66	10.73	7.66
3/a (super-GTO, ballistic)	4.98	10.93	28.79	10.93
3/b (super-GTO, low-thrust)	3.00	8.07	10.13	7.05

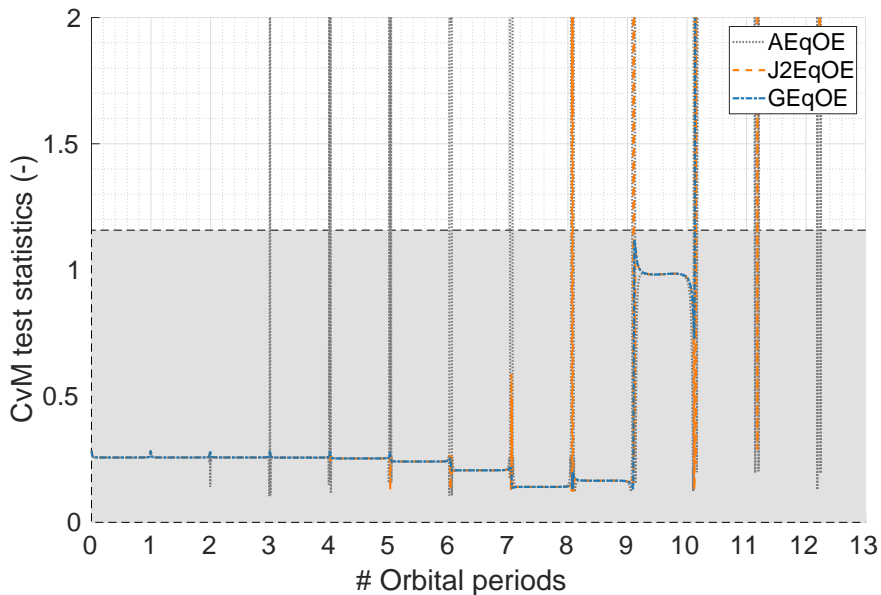


Figure 7: CvM test statistics for Case 3 (low-thrust).

The six scenarios are summarized in Table 3. The last column displays the UR obtained by including in the potential energy only the  $J_2$  term of GEqOE. This result, not shown in the plots for clarity, highlights the benefit of embedding higher order terms of the geopotential into the definition of GEqOE especially for high eccentricity orbits where the improvement in realism can be dramatic.

## 7 Conclusions

A new linear uncertainty propagation scheme based on a set of generalized equinoctial orbital elements (GEqOE) has been proposed and shown to be superior, in terms of uncertainty realism (UR), to all other linear propagation methods proposed so far. A UR improvement, computed with a Mahalanobis distance

Cramér-von Mises test, of more than at least 36% is obtained, compared to the use of J2 equinoctial orbital elements (J2EqOE), for different classes of ballistic Earth orbits. A key result of the article concerns the influence of higher order geopotential harmonics in degrading UR and the possibility of drastically reducing this effect by the use of GEqOE. It is seen that when harmonics terms of higher order than  $J_2$  are embedded in the definition of the GEqOE, a considerable improvement in UR is observed for all Earth-orbiting scenarios analyzed. The improvement becomes dramatic when highly eccentric orbits are considered. Finally, the analysis of the impact of a continuous tangential low-thrust acceleration on the UR of different classes of Earth orbits considering full-thrust capability of state-of-the-art electric propulsion systems suggests a small, although not negligible reduction in UR for all cases. Nevertheless, GEqOE retain their advantage over competing sets of elements even for low-thrust-perturbed orbits.

While the GEqOE uncertainty propagation scheme investigated in this article employs a linear model for maximum computation efficiency, nonlinear techniques can be applied to the same set of elements to further improve the UR at the expense of a reduced computation efficiency.

## Acknowledgments

This work was supported by MINECO/AEI and FEDER/EU under Project PID2020-112576GB-C21. The authors thank the MINECO/AEI of Spain for their financial support.

Alicia Martínez-Cacho, of Universidad Politécnica de Madrid (UPM), was supported by a PhD grant under UPM “Programa Propio”.

The views expressed are those of the authors and do not necessarily represent the views of the ispace-inc.

## References

- [1] P. S. Maybeck, *Stochastic models, estimation, and control Volume 2*, Vol. 141-2 of *Mathematics in Science and Engineering*. New York: Academic press, 1982.
- [2] R. Armellin, P. Di Lizia, F. Bernelli-Zazzera, and M. Berz, “Asteroid close encounters characterization using differential algebra: the case of Apophis,” *Celestial Mechanics and Dynamical Astronomy*, Vol. 107, No. 4, 2010, pp. 451–470, 10.1007/s10569-010-9283-5.
- [3] R. S. Park and D. J. Scheeres, “Nonlinear mapping of Gaussian statistics: theory and applications to spacecraft trajectory design,” *Journal of Guidance, Control, and Dynamics*, Vol. 29, No. 6, 2006, pp. 1367–1375, 10.2514/1.2017.

- [4] J. Roa and R. S. Park, “Reduced Nonlinear Model for Orbit Uncertainty Propagation and Estimation,” *Journal of Guidance, Control, and Dynamics*, 2021, pp. 1–15, 10.2514/1.G005519.
- [5] D. Giza, P. Singla, and M. Jah, “An Approach for Nonlinear Uncertainty Propagation: Application to Orbital Mechanics,” *AIAA Guidance, Navigation, and Control Conference*, No. 2009-6082, Chicago, Illinois, 10-13 August 2009, 10.2514/6.2009-6082.
- [6] G. Terejanu, P. Singla, T. Singh, and P. D. Scott, “Uncertainty Propagation for Nonlinear Dynamic Systems Using Gaussian Mixture Models,” *Journal of Guidance, Control, and Dynamics*, Vol. 31, No. 6, 2008, pp. 1623–1633, 10.2514/1.36247.
- [7] S. J. Julier and J. K. Uhlmann, “New extension of the Kalman filter to nonlinear systems,” *Signal processing, sensor fusion, and target recognition VI*, Vol. 3068, International Society for Optics and Photonics, 1997, pp. 182–193, 10.1117/12.280797.
- [8] B. A. Jones, A. Doostan, and G. H. Born, “Nonlinear Propagation of Orbit Uncertainty Using Non-Intrusive Polynomial Chaos,” *Journal of Guidance, Control, and Dynamics*, Vol. 36, No. 2, 2013, pp. 430–444, 10.2514/1.57599.
- [9] A. Milani, M. E. Sansaturio, G. Tommei, O. Arratia, and S. R. Chesley, “Multiple solutions for asteroid orbits: computational procedure and applications,” *Astronomy & Astrophysics*, Vol. 431, No. 2, 2005, pp. 729–746, 10.1051/0004-6361:20041737.
- [10] C. Tardioli, M. Kubicek, M. Vasile, E. Minisci, and A. Riccardi, “Comparison of non-intrusive approaches to uncertainty propagation in orbital mechanics,” *AAS/AIAA Astrodynamics Specialist Conference 2015*, No. AAS 15-545, Vail, California, American Astronautical Society, 2015, pp. 3979–3992.
- [11] V. Vittaldev, R. P. Russell, and R. Linares, “Spacecraft Uncertainty Propagation Using Gaussian Mixture Models and Polynomial Chaos Expansions,” *Journal of Guidance, Control, and Dynamics*, Vol. 39, No. 12, 2016, pp. 2615–2626, 10.2514/1.G001571.
- [12] J. L. Junkins, M. R. Akella, and K. T. Alfriend, “Non-Gaussian error propagation in orbital mechanics,” *The Journal Of the Astronautical Sciences*, Vol. 44(4), 1996, pp. 541–563.
- [13] C. Sabol, T. Sukut, K. Hill, K. T. Alfriend, B. Wright, Y. Li, and P. Schumacher, “Linearized orbit covariance generation and propagation analysis via simple Monte Carlo simulations,” *AAS 10-134, AAS/AIAA Space Flight Mechanics Conference*, San Diego, CA, February, 2010, pp. 14–17.

- [14] Z. Folcik, A. Lue, and J. Vatsky, “Reconciling covariances with reliable orbital uncertainty,” *12th Advanced Maui Optical and Space Surveillance Technologies Conference*, 2011.
- [15] J. Hernando-Ayuso and C. Bombardelli, “Orbit covariance propagation via quadratic-order state transition matrix in curvilinear coordinates,” *Celestial Mechanics and Dynamical Astronomy*, Vol. 129, Sep 2017, pp. 215–234, 10.1007/s10569-017-9773-9.
- [16] V. T. Coppola and S. Tanygin, “Using Bent Ellipsoids to Represent Large Position Covariance in Orbit Propagation,” *Journal of Guidance, Control, and Dynamics*, Vol. 38, No. 9, 2015, pp. 1775–1784, 10.2514/1.G001011.
- [17] R. G. Melton, “Time-Explicit Representation of Relative Motion Between Elliptical Orbits,” *Journal of Guidance, Control, and Dynamics*, Vol. 23, No. 4, 2000, pp. 604–610, 10.2514/2.4605.
- [18] C. M. Lane and P. Axelrad, “Formation Design in Eccentric Orbits Using Linearized Equations of Relative Motion,” *Journal of Guidance, Control, and Dynamics*, Vol. 29, No. 1, 2006, pp. 146–160, 10.2514/1.13173.
- [19] K. Hill, K. Alfriend, and C. Sabol, “Covariance-based uncorrelated track association,” *AIAA/AAS Astrodynamics Specialist Conference*, No. AIAA 2008-7211, Honolulu, Hawaii, 18-21 August 2008.
- [20] L. M. Weis, “Uncertainty in KS Space with Arbitrary Forces,” *AIAA SciTech Forum*, American Institute of Aeronautics and Astronautics, Jan. 2018, 10.2514/6.2018-0728.
- [21] J. Roa Vicens and J. Peláez Álvarez, “Efficient trajectory propagation for orbit determination problems,” *AAS/AIAA Astrodynamics Specialist Conference*, No. AAS-15-730, Vail, Colorado, USA, Univelt, August 2015.
- [22] J. M. Aristoff, J. T. Horwood, and K. T. Alfriend, “On a set of  $J_2$  equinoctial orbital elements and their use for uncertainty propagation,” *Celestial Mechanics and Dynamical Astronomy*, Vol. 133, No. 9, 2021, pp. 1–19, 10.1007/s10569-021-10004-0.
- [23] G. Baù, J. Hernando-Ayuso, and C. Bombardelli, “A generalization of the equinoctial orbital elements,” *Celestial Mechanics and Dynamical Astronomy*, Vol. 133, No. 50, 2021, 10.1007/s10569-021-10049-1.
- [24] J. L. Arsenault, K. C. Ford, and P. E. Koskela, “Orbit Determination Using Analytic Partial Derivatives of Perturbed Motion,” *AIAA Journal*, Vol. 8, No. 1, 1970, pp. 4–9, 10.2514/3.5597.
- [25] R. A. Broucke and P. J. Cefola, “On the equinoctial orbit elements,” *Celestial Mechanics*, Vol. 5, 1972, pp. 303–310, 10.1007/BF01228432.

- [26] J. T. Horwood, N. D. Aragon, and A. B. Poore, “Gaussian Sum Filters for Space Surveillance: Theory and Simulations,” *Journal of Guidance, Control, and Dynamics*, Vol. 34, November 2011, pp. 1839–1851, 10.2514/1.53793.
- [27] R. Battin, *An Introduction to the Mathematics and Methods of Astrodynamics*. Reston, Virginia: AIAA, 1999.
- [28] D. Brouwer, “Solution of the problem of artificial satellite theory without drag,” *The Astronomical Journal*, Vol. 64, 1959, p. 378, 10.1086/107958.
- [29] P. Abbasrezaee, M. Mirshams, and S. Seyed-Zamani, “Conceptual GEO Telecommunication All-Electric Satellite Design Based on Statistical Model,” *2019 9th International Conference on Recent Advances in Space Technologies (RAST)*, IEEE, 2019, pp. 503–507, 10.1109/RAST.2019.8767854.
- [30] J. Ries, S. Bettadpur, R. Eanes, Z. Kang, U. Ko, C. McCullough, P. Nagel, N. Pie, S. Poole, T. Richter, *et al.*, “Development and Evaluation of the Global Gravity Model GGM05-CSR-16-02,” *Center for Space Research, Univ. of Texas at Austin TR CSR-16-02, Austin, TX*, 2016.
- [31] L. E. Cunningham, “On the computation of the spherical harmonic terms needed during the numerical integration of the orbital motion of an artificial satellite,” *Celestial Mechanics*, Vol. 2, No. 2, 1970, pp. 207–216, 10.1007/BF01229495.
- [32] G. Métris, J. Xu, and I. Wytrzyszczak, “Derivatives of the gravity potential with respect to rectangular coordinates,” *Celestial Mechanics and Dynamical Astronomy*, Vol. 71, No. 2, 1998, pp. 137–151, 10.1023/A:1008361202235.
- [33] E. Fantino and S. Casotto, “Methods of harmonic synthesis for global geopotential models and their first-, second- and third-order gradients,” *Journal of Geodesy*, Vol. 83, No. 7, 2009, pp. 595–619, 10.1007/s00190-008-0275-0.

## A Computation of $\partial\mathbf{f}/\partial\mathbf{y}$

In the following, the elements of the  $6 \times 6$  matrix  $\partial\mathbf{f}/\partial\mathbf{y}$  are computed, where  $\mathbf{f}(\mathbf{y}, t)$  and  $\mathbf{y}$  have been introduced in Section 4. For this purpose, it is useful to define the function  $\mathbf{f}(\mathbf{y}, \mathbf{a}, \mathbf{b}, t)$ :

$$\mathbf{f}(\mathbf{y}, \mathbf{a}(\mathbf{y}, t), \mathbf{b}(\mathbf{y}, t), t) = \mathbf{f}(\mathbf{y}, t),$$

where

$$\mathbf{a} = (r, u, h, c, L)^T,$$

$$\mathbf{b} = (\mathcal{U}_t, P_r, P_f, F_h, S)^T,$$

with

$$U_t = \frac{\partial \mathcal{U}}{\partial t}, \quad S = 2\mathcal{U} - rF_r.$$

Recall that  $L$  is the true longitude (Eq. 8) and  $F_r, F_h, P_r, P_f$  are defined in Eq. (20).

The components of  $\mathbf{f}$  are given by equations (11)–(16). One has

$$\frac{\partial \mathbf{f}}{\partial \mathbf{y}} = \frac{\partial \mathbf{f}}{\partial \mathbf{y}} + \frac{\partial \mathbf{f}}{\partial \mathbf{a}} \frac{\partial \mathbf{a}}{\partial \mathbf{y}} + \frac{\partial \mathbf{f}}{\partial \mathbf{b}} \frac{\partial \mathbf{b}}{\partial \mathbf{y}}. \quad (38)$$

The following subsections deal with the computation of the matrices that appear on the right-hand side of (38).

It is useful to define the quantities

$$\sigma_1 = p_2 + \cos L,$$

$$\sigma_2 = p_1 + \sin L,$$

$$\sigma_3 = \sin L + \zeta \sigma_1,$$

$$\sigma_4 = \cos L + \zeta \sigma_2,$$

$$\zeta = \frac{r}{\varrho},$$

$$\tilde{\zeta} = 1 + \frac{r}{\varrho},$$

where  $\varrho$  is defined in (18).



## A.1 $\partial \mathbf{f} / \partial \mathbf{y}$

The six rows of this matrix are given by<sup>4</sup>:

$$\begin{aligned}\frac{\partial \mathbf{f}_1}{\partial \mathbf{y}} &= - \left( \frac{1}{\mu\nu} \right)^{2/3} \dot{\epsilon} (1, 0, 0, 0, 0, 0), \\ \frac{\partial \mathbf{f}_2}{\partial \mathbf{y}} &= \left( \frac{2X}{3\mu\beta} S, \frac{r^2}{c^2} \dot{\epsilon}, \frac{h-c}{r^2} - \frac{\gamma}{h} F_h + \frac{2}{c} S, 0, -\frac{Xp_2}{h} F_h, \frac{Yp_2}{h} F_h \right), \\ \frac{\partial \mathbf{f}_3}{\partial \mathbf{y}} &= \left( -\frac{2Y}{3\mu\beta} S, \frac{\gamma}{h} F_h - \frac{h-c}{r^2} - \frac{2}{c} S, \frac{r^2}{c^2} \dot{\epsilon}, 0, \frac{Xp_1}{h} F_h, -\frac{Yp_1}{h} F_h \right), \\ \frac{\partial \mathbf{f}_4}{\partial \mathbf{y}} &= \left( 1 - \frac{2\alpha r}{3\mu\beta} S, \frac{\partial \mathbf{f}_4}{\partial p_1}, \frac{\partial \mathbf{f}_4}{\partial p_2}, 0, -\frac{X}{h} F_h, \frac{Y}{h} F_h \right), \\ \frac{\partial \mathbf{f}_5}{\partial \mathbf{y}} &= \left( 0, 0, 0, 0, \frac{Yq_1}{h} F_h, \frac{Yq_2}{h} F_h \right), \\ \frac{\partial \mathbf{f}_6}{\partial \mathbf{y}} &= \left( 0, 0, 0, 0, \frac{Xq_1}{h} F_h, \frac{Xq_2}{h} F_h \right),\end{aligned}$$

where

$$\frac{\partial \mathbf{f}_4}{\partial p_i} = \left[ \frac{ruc}{\mu^2} \zeta \dot{\epsilon} + \left( 1 - \frac{r}{a} - \frac{1}{\alpha^2} \right) \frac{S}{c} \right] \frac{\alpha^2 p_i}{\beta}, \quad i = 1, 2.$$

The definitions of  $X, Y$  are given in (17) and those of  $\gamma, \alpha, \beta$  in (19).

## A.2 $\partial \mathbf{f} / \partial \mathbf{a}$

The six rows of this matrix are given by:

1<sup>st</sup> row

$$\frac{\partial \mathbf{f}_1}{\partial \mathbf{a}} = -3 \left( \frac{\nu}{\mu^2} \right)^{1/3} \left( -\frac{h}{r^2} P_f, P_r, \frac{1}{r} P_f, 0, 0 \right);$$

---

<sup>4</sup>Here  $Y_i$  denotes the  $i$ -th component of the vector  $\mathbf{Y}$ .

2<sup>nd</sup> row

$$\frac{\partial \mathbf{f}_2}{\partial a_1} = - \left[ \frac{2(h-c)}{r^2} + \frac{\gamma}{h} F_h \right] \frac{p_2}{r} + \frac{\cos L}{ca} S + \frac{1}{\mu} [\sigma_3 (\mathcal{U}_t + u P_r) + \varsigma \sigma_2 \dot{\mathcal{E}}],$$

$$\frac{\partial \mathbf{f}_2}{\partial a_2} = \frac{r \sigma_3}{\mu} P_r,$$

$$\frac{\partial \mathbf{f}_2}{\partial a_3} = \left( \frac{1}{r^2} + \frac{\gamma}{h^2} F_h \right) p_2 + \frac{\sigma_3}{\mu} P_f,$$

$$\frac{\partial \mathbf{f}_2}{\partial a_4} = -\frac{p_2}{r^2} - \frac{1}{c^2} \left[ \left( \frac{X}{a} + 2p_2 \right) S + \frac{2r^2 \sigma_2}{c} \dot{\mathcal{E}} \right],$$

$$\frac{\partial \mathbf{f}_2}{\partial a_5} = (q_1 \sin L + q_2 \cos L) \frac{r p_2}{h} F_h - \frac{Y}{ca} S + \frac{X \zeta}{\mu} \dot{\mathcal{E}};$$

3<sup>rd</sup> row

$$\frac{\partial \mathbf{f}_3}{\partial a_1} = \left[ \frac{2(h-c)}{r^2} + \frac{\gamma}{h} F_h \right] \frac{p_1}{r} - \frac{\sin L}{ca} S + \frac{1}{\mu} [\sigma_4 (\mathcal{U}_t + u P_r) + \varsigma \sigma_1 \dot{\mathcal{E}}],$$

$$\frac{\partial \mathbf{f}_3}{\partial a_2} = \frac{r \sigma_4}{\mu} P_r,$$

$$\frac{\partial \mathbf{f}_3}{\partial a_3} = - \left( \frac{1}{r^2} + \frac{\gamma}{h^2} F_h \right) p_1 + \frac{\sigma_4}{\mu} P_f,$$

$$\frac{\partial \mathbf{f}_3}{\partial a_4} = \frac{p_1}{r^2} + \frac{1}{c^2} \left[ \left( \frac{Y}{a} + 2p_1 \right) S - \frac{2r^2 \sigma_1}{c} \dot{\mathcal{E}} \right],$$

$$\frac{\partial \mathbf{f}_3}{\partial a_5} = -(q_1 \sin L + q_2 \cos L) \frac{r p_1}{h} F_h - \frac{X}{ca} S - \frac{Y \zeta}{\mu} \dot{\mathcal{E}};$$

4<sup>th</sup> row

$$\frac{\partial \mathbf{f}_4}{\partial a_1} = -\frac{2(h-c)}{r^3} - \frac{\gamma}{rh} F_h + \frac{uc\alpha}{\mu^2} \left[ \zeta (\mathcal{U}_t + u P_r) + \varsigma \dot{\mathcal{E}} \right] - \frac{\alpha}{ca} S,$$

$$\frac{\partial \mathbf{f}_4}{\partial a_2} = \frac{rc\alpha}{\mu^2} \zeta (\dot{\mathcal{E}} + u P_r),$$

$$\frac{\partial \mathbf{f}_4}{\partial a_3} = \frac{1}{r^2} + \frac{\gamma}{h^2} F_h + \frac{uc\alpha}{\mu^2} \zeta P_f,$$

$$\frac{\partial \mathbf{f}_4}{\partial a_4} = -\frac{1}{r^2} + \frac{ru\alpha}{\mu^2} (1-\varsigma) \dot{\mathcal{E}} - \left[ \frac{1}{\alpha} + \alpha \left( 1 - \frac{r}{a} \right) \right] \frac{S}{c^2},$$

$$\frac{\partial \mathbf{f}_4}{\partial a_5} = \frac{r}{h} (q_1 \sin L + q_2 \cos L) F_h;$$

5<sup>th</sup> row

$$\frac{\partial f_5}{\partial \mathbf{a}} = \frac{F_h}{2h} (1 + q_1^2 + q_2^2) \left( \sin L, 0, -\frac{Y}{h}, 0, X \right);$$

6<sup>th</sup> row

$$\frac{\partial f_6}{\partial \mathbf{a}} = \frac{F_h}{2h} (1 + q_1^2 + q_2^2) \left( \cos L, 0, -\frac{X}{h}, 0, -Y \right).$$

### A.3 $\partial \mathbf{a} / \partial \mathbf{y}$

The five rows of this matrix are given by:

1<sup>st</sup> row

$$\frac{\partial a_1}{\partial \mathbf{y}} = \left( -\frac{2r}{3\nu}, -\frac{u}{\nu} \cos \mathcal{K} - a \sin \mathcal{K}, \frac{u}{\nu} \sin \mathcal{K} - a \cos \mathcal{K}, \frac{u}{\nu}, 0, 0 \right);$$

2<sup>nd</sup> row

$$\begin{aligned} \frac{\partial a_2}{\partial \mathbf{y}} = & \left( \frac{u}{3\nu}, \frac{1}{r\nu} \left( u^2 - \frac{\mu}{r} \right) \cos \mathcal{K} + \frac{ua}{r} \sin \mathcal{K}, \frac{1}{r\nu} \left( \frac{\mu}{r} - u^2 \right) \sin \mathcal{K} \right. \\ & \left. + \frac{ua}{r} \cos \mathcal{K}, \frac{\sqrt{\mu a}}{r} \left( \frac{a}{r} - 1 \right) - \frac{u^2}{r\nu}, 0, 0 \right); \end{aligned}$$

3<sup>rd</sup> row

$$\frac{\partial a_3}{\partial \mathbf{y}} = \frac{1}{h} \left( c \frac{\partial a_4}{\partial \mathbf{y}} - 2r \mathcal{U} \frac{\partial a_1}{\partial \mathbf{y}} - r^2 \frac{\partial \mathcal{U}}{\partial \mathbf{y}} \right);$$

4<sup>th</sup> row

$$\frac{\partial a_4}{\partial \mathbf{y}} = \left( -\frac{a^2 \beta}{3}, -\left( \frac{\mu^2}{\nu} \right)^{1/3} \frac{p_1}{\beta}, -\left( \frac{\mu^2}{\nu} \right)^{1/3} \frac{p_2}{\beta}, 0, 0, 0 \right);$$

5<sup>th</sup> row

$$\begin{aligned}\frac{\partial a_5}{\partial \nu} &= \frac{\partial a_5}{\partial q_1} = \frac{\partial a_5}{\partial q_2} = 0, \\ \frac{\partial a_5}{\partial p_1} &= \frac{a}{r} \left[ \alpha \left( \frac{a}{r} \cos \mathcal{K} - \frac{ru\alpha p_1}{c} \right) \left( \frac{1}{\zeta} - 1 \right) - \frac{Yu\alpha}{\sqrt{\mu a}} \right. \\ &\quad \left. - \cos L - \frac{a}{r} \cos \mathcal{K} \cos(L - \mathcal{K}) \right], \\ \frac{\partial a_5}{\partial p_2} &= \frac{a}{r} \left[ -\alpha \left( \frac{a}{r} \sin \mathcal{K} + \frac{ru\alpha p_2}{c} \right) \left( \frac{1}{\zeta} - 1 \right) - \frac{Xu\alpha}{\sqrt{\mu a}} \right. \\ &\quad \left. + \sin L + \frac{a}{r} \sin \mathcal{K} \cos(L - \mathcal{K}) \right], \\ \frac{\partial a_5}{\partial \mathcal{L}} &= \frac{a^2}{r^2} \left[ \alpha \left( \frac{r}{a} - 1 \right) \left( \frac{1}{\zeta} - 1 \right) + \cos(L - \mathcal{K}) \right].\end{aligned}$$

The quantity  $\mathcal{K}$  can be computed as described in [23], Sect. 4. For the computation of  $\partial \mathcal{U} / \partial \mathbf{y}$  see Sect. A.5.

#### A.4 $\partial \mathbf{f} / \partial \mathbf{b}$

The six rows of this matrix are given by:

1<sup>st</sup> row

$$\frac{\partial \mathbf{f}_1}{\partial \mathbf{b}} = -3 \left( \frac{\nu}{\mu^2} \right)^{1/3} \left( 1, u, \frac{h}{r}, 0, 0 \right);$$

2<sup>nd</sup> row

$$\frac{\partial \mathbf{f}_2}{\partial \mathbf{b}} = \left( \frac{r}{\mu} \sigma_3, \frac{ru}{\mu} \sigma_3, \frac{h}{\mu} \sigma_3, -\frac{\gamma p_2}{h}, \frac{1}{c} \left( \frac{X}{a} + 2p_2 \right) \right);$$

3<sup>rd</sup> row

$$\frac{\partial \mathbf{f}_3}{\partial \mathbf{b}} = \left( \frac{r}{\mu} \sigma_4, \frac{ru}{\mu} \sigma_4, \frac{h}{\mu} \sigma_4, \frac{\gamma p_1}{h}, -\frac{1}{c} \left( \frac{Y}{a} + 2p_1 \right) \right);$$

4<sup>th</sup> row

$$\frac{\partial \mathbf{f}_4}{\partial \mathbf{b}} = \left( \frac{ru\alpha}{\mu^2} \zeta, \frac{ru^2\alpha}{\mu^2} \zeta, \frac{uhc\alpha}{\mu^2} \zeta, -\frac{\gamma}{h}, \frac{1}{c} \left[ \frac{1}{\alpha} + \alpha \left( 1 - \frac{r}{a} \right) \right] \right);$$

5<sup>th</sup> row

$$\frac{\partial f_5}{\partial \mathbf{b}} = \left( 0, 0, 0, \frac{Y}{2h}(1 + q_1^2 + q_2^2), 0 \right);$$

6<sup>th</sup> row

$$\frac{\partial f_6}{\partial \mathbf{b}} = \left( 0, 0, 0, \frac{X}{2h}(1 + q_1^2 + q_2^2), 0 \right).$$

## A.5 $\partial \mathbf{b} / \partial \mathbf{y}$

Let

$$\mathbf{x} = (x, y, z, \dot{x}, \dot{y}, \dot{z})^T$$

be the set of Cartesian coordinates of the position  $\mathbf{r}$  and velocity  $\dot{\mathbf{r}}$  of the propagated body with respect to an inertial reference frame  $\Sigma$ . In order to compute  $\partial \mathbf{b} / \partial \mathbf{y}$  the chain rule is applied:

$$\frac{\partial \mathbf{b}}{\partial \mathbf{y}} = \frac{\partial \mathbf{b}}{\partial \mathbf{x}} \frac{\partial \mathbf{x}}{\partial \mathbf{y}}.$$

Note that the matrix  $\partial \mathbf{x} / \partial \mathbf{y}$  is provided in [23], Sect. 6.1. The first row of the matrix  $\partial \mathbf{b} / \partial \mathbf{x}$  is

$$\frac{\partial b_1}{\partial \mathbf{x}} = \left( \frac{\partial \mathcal{U}_t}{\partial \mathbf{r}}, 0, 0, 0 \right).$$

Regarding the other rows one has:

2<sup>nd</sup> row

$$\frac{\partial b_2}{\partial \mathbf{x}} = \mathbf{e}_r^T \frac{\partial \mathbf{P}}{\partial \mathbf{x}} + \mathbf{P}^T \frac{\partial \mathbf{e}_r}{\partial \mathbf{x}},$$

3<sup>rd</sup> row

$$\frac{\partial b_3}{\partial \mathbf{x}} = \mathbf{e}_f^T \frac{\partial \mathbf{P}}{\partial \mathbf{x}} + \mathbf{P}^T \frac{\partial \mathbf{e}_f}{\partial \mathbf{x}},$$

4<sup>th</sup> row

$$\frac{\partial b_4}{\partial \mathbf{x}} = \mathbf{e}_h^T \frac{\partial \mathbf{F}}{\partial \mathbf{x}} + \mathbf{F}^T \frac{\partial \mathbf{e}_h}{\partial \mathbf{x}},$$

5<sup>th</sup> row

$$\frac{\partial b_5}{\partial \mathbf{x}} = 2 \frac{\partial \mathcal{U}}{\partial \mathbf{x}} - \frac{\partial r}{\partial \mathbf{x}} F_r - r \left( \mathbf{e}_r^T \frac{\partial \mathbf{F}}{\partial \mathbf{x}} + \mathbf{F}^T \frac{\partial \mathbf{e}_r}{\partial \mathbf{x}} \right),$$

where the two vectors  $\mathbf{F}$  and  $\mathbf{P}$  (introduced in Eqs. 1, 2) are expressed in  $\Sigma$  and

$$\frac{\partial r}{\partial \mathbf{x}} = (\mathbf{e}_r^T, 0, 0, 0),$$

$$\begin{aligned}
\frac{\partial \mathbf{e}_r}{\partial \mathbf{r}} &= -\frac{1}{r^3} R^2, & \frac{\partial \mathbf{e}_r}{\partial \dot{\mathbf{r}}} &= O_3, \\
\frac{\partial \mathbf{e}_f}{\partial \mathbf{r}} &= \frac{1}{rh} \left( \frac{u}{r} R^2 + \frac{1}{h^2} HCH^T \right), & \frac{\partial \mathbf{e}_f}{\partial \dot{\mathbf{r}}} &= -\frac{1}{rh} \left( R^2 + \frac{1}{h^2} HBH^T \right), \\
\frac{\partial \mathbf{e}_h}{\partial \mathbf{r}} &= \frac{1}{h^2} (H\dot{\mathbf{r}}) \mathbf{e}_h^T, & \frac{\partial \mathbf{e}_h}{\partial \dot{\mathbf{r}}} &= -\frac{r}{h} \mathbf{e}_f \mathbf{e}_h^T,
\end{aligned}$$

with  $O_3, I_3$  denoting the null and identity  $3 \times 3$  matrices, respectively, and

$$R = \begin{pmatrix} 0 & -z & y \\ z & 0 & -x \\ -y & x & 0 \end{pmatrix}, \quad H = \begin{pmatrix} 0 & -h_3 & h_2 \\ h_3 & 0 & -h_1 \\ -h_2 & h_1 & 0 \end{pmatrix},$$

$$C = \dot{\mathbf{r}} \mathbf{r}^T, \quad B = \mathbf{r} \mathbf{r}^T,$$

$$h_1 = y\dot{z} - z\dot{y}, \quad h_2 = z\dot{x} - x\dot{z}, \quad h_3 = x\dot{y} - y\dot{x}.$$

Moreover, for a generic vector  $\mathbf{Y}$  one has

$$\frac{\partial \mathbf{Y}}{\partial \mathbf{x}} = \left( \frac{\partial \mathbf{Y}}{\partial \mathbf{r}} \mid \frac{\partial \mathbf{Y}}{\partial \dot{\mathbf{r}}} \right).$$

Finally, assuming that  $\mathcal{U}$  is a function of  $\mathbf{r}$  and possibly of time, one has

$$\frac{\partial \mathcal{U}}{\partial \mathbf{y}} = \frac{\partial \mathcal{U}}{\partial \mathbf{r}} \frac{\partial \mathbf{r}}{\partial \mathbf{y}},$$

where  $\partial \mathbf{r} / \partial \mathbf{y}$  is given in [23], Sect. 6.1.

## B Secular evolution of $\mathcal{L}$ under the effect of $\mathbf{J}_2$

From Eqs. (33), (34) one can write, for an equatorial orbit

$$\dot{\mathcal{L}} = \nu_0 + \frac{J_2 \mu R^2}{2cr^3} \left[ 1 + \frac{1}{\alpha} + \alpha \left( 1 - \frac{r}{a_0} \right) \right], \quad (39)$$

where terms of order higher than one in  $\mathbf{J}_2$  have been neglected in Eq. (34). Let the mean value of the eccentricity  $e$  be equal to zero. Then, from Eq. (4) one can assume that the mean generalized eccentricity is

also zero, which implies  $\alpha = 1/2$ ,  $c = \sqrt{\mu a_0}$ ,  $r = a_0$ . After applying these substitutions, Eq. (39) reduces to

$$\dot{\mathcal{L}} = \nu_0 + \frac{3J_2\mu R^2}{2a_0^3\sqrt{\mu a_0}},$$

where the symbol  $\dot{\mathcal{L}}$  denotes now the secular rate of the generalized mean longitude. Using the first relation in (18) and the definition of  $A$  in (29) one finds

$$\dot{\mathcal{L}} = \nu_0 + \frac{3J_2R^2\nu_0^{7/3}}{2\mu^{2/3}} = \nu_0(1 + J_2A\nu_0^{4/3}),$$

which can be integrated to give Eq. (35).

## C Partial derivatives of the spherical harmonics potential

Multiple algorithms exist to compute the potential of the spherical harmonics perturbation and its derivatives. A non-exhaustive list includes the methods of Legendre, Clenshaw, Pines and the one used in this work, Cunningham-Metris. A comparison of these methods is presented in [33]. All of them are naturally defined in ECEF coordinates, and can provide the potential and its first and second derivatives with respect to the ECEF Cartesian position. In order to propagate the orbital state and the state transition matrix in the GEqOE space one has to compute

$$\frac{\partial \mathcal{U}}{\partial \mathbf{r}_{\text{ECI}}}, \quad \frac{\partial \mathcal{U}}{\partial t}, \quad \frac{\partial^2 \mathcal{U}}{\partial \mathbf{r}_{\text{ECI}}^2}, \quad \frac{\partial}{\partial \mathbf{r}_{\text{ECI}}} \left( \frac{\partial \mathcal{U}}{\partial t} \right), \quad (40)$$

where  $\mathbf{r}_{\text{ECI}}$  denotes the position of the propagated body expressed in the Earth-centered inertial frame (ECI). The first two terms in (40) appear in the equations of motion, while the other two are needed for the propagation of the state transition matrix.

The Cartesian state vector  $\mathbf{x}$  can be rotated from ECI to ECEF as

$$\mathbf{x}_{\text{ECEF}} = \begin{bmatrix} \mathfrak{R}(t) & O_3 \\ \dot{\mathfrak{R}}(t) & \mathfrak{R}(t) \end{bmatrix} \mathbf{x}_{\text{ECI}},$$

where  $\mathfrak{R}$  is the rotation matrix from ECI to ECEF and  $O_3$  is the  $3 \times 3$  null matrix.

The first term in (40) is used to calculate  $\mathbf{F}$ :

$$\frac{\partial \mathcal{U}}{\partial \mathbf{r}_{\text{ECI}}} = \frac{\partial \mathcal{U}}{\partial \mathbf{r}_{\text{ECEF}}} \mathfrak{R}.$$

The second term can be obtained as the time derivative of  $\mathcal{U}(t) = \mathcal{U}(\mathbf{r}_{\text{ECI}}(t))$  after expressing the ECI position in ECEF coordinates:

$$\frac{\partial \mathcal{U}}{\partial t} = \frac{\partial \mathcal{U}}{\partial \mathbf{r}_{\text{ECEF}}} \dot{\mathfrak{R}} \mathfrak{R}^T \mathbf{r}_{\text{ECEF}}.$$

The third term contributes to  $\partial \mathbf{F} / \partial \mathbf{x}$  in Section A.5, and reads

$$\frac{\partial^2 \mathcal{U}}{\partial \mathbf{r}_{\text{ECI}}^2} = \mathfrak{R}^T \frac{\partial^2 \mathcal{U}}{\partial \mathbf{r}_{\text{ECEF}}^2} \mathfrak{R}.$$

The last term in (40), which is the first component of  $\partial b_1 / \partial \mathbf{x}$  (see Sect. A.5), is given by

$$\frac{\partial}{\partial \mathbf{r}_{\text{ECI}}} \left( \frac{\partial \mathcal{U}}{\partial t} \right) = \mathfrak{R}^T \frac{\partial^2 \mathcal{U}}{\partial \mathbf{r}_{\text{ECEF}}^2} \dot{\mathfrak{R}} \mathfrak{R}^T \mathbf{r}_{\text{ECEF}} + \frac{\partial \mathcal{U}}{\partial \mathbf{r}_{\text{ECEF}}} \dot{\mathfrak{R}}.$$